



ELSEVIER

Atmospheric Research 66 (2003) 123–139

ATMOSPHERIC
RESEARCH

www.elsevier.com/locate/atmos

The effects of a river valley on an isolated cumulonimbus cloud development

Mladjen Ćurić*, Dejan Janc, Dragana Vujović, Vladan Vučković

Institute of Meteorology, University of Belgrade, PO Box 368, Belgrade 11000, Yugoslavia

Received 14 December 2001; received in revised form 6 August 2002; accepted 3 September 2002

Abstract

The mechanism of development, propagation and front-side cell regeneration of a three-dimensional isolated cumulonimbus (Cb) cloud is investigated by a cloud-resolving mesoscale model. Interactions of the simulated storm with orography including a river valley were studied. According to observational evidence, the mountainous environment of the Western Morava valley (Serbia) is an important place for the formation of isolated Cb clouds. Once formed, they move down into the valley and continue to propagate along it.

The effects of orography on the development, propagation and regeneration of the model Cb cloud are recognized by comparison of its development with that simulated over flat terrain under the same conditions. In our study, two cases are considered: complex terrain case (referred to CT case) and flat terrain case (referred to FT case). It is found that:

- Orography effects (CT case) play an important role on Cb cloud life; the cloud propagation and development are inhibited in lateral direction and its form is more compact. Cold air outflow near the ground remains in the valley with an increased depth compared to the FT case. Warm environmental air approaching the cold air nose from the opposite direction is forced aloft more frequently than in the FT case. As a consequence, the simulated cloud propagates faster in this case.
- Warm environmental air forcing over cold air nose in the FT case is stronger initially than in the CT case, since the cloud development is not prevented by orography from the lateral direction. Consequently, the cold air outflow is more intense. In contrast, the cloud regenerates more slowly, since the cold air diverges in all directions, which in turn, makes the cold air nose thinner. The alternate reform and collapse of the cold air nose are more expressed in the CT case.

© 2002 Elsevier Science B.V. All rights reserved.

Keywords: Mesoscale model; Cumulonimbus development; Orography effects; Cell regeneration; River valley effects

* Corresponding author. Fax: +381-11-3282-619.

E-mail address: curic@ff.bg.ac.yu (M. Ćurić).

1. Introduction

Three-dimensional numerical simulations of convective clouds have been a subject of increased interest during the past three decades. The significant attention was given to the modeling of both dynamics and microphysics. Cloud models have become capable to reproduce well many observational characteristics of clouds such as the relationship between environmental winds and rotation inside a cloud, updraft and downdraft orientation, cloud motion relative to the mean environmental wind direction and environmental wind flow around a cloud (Klemp and Wilhelmson, 1978; Toutenhoofd and Klemp, 1983; Rotunno et al., 1988; Droegemeier and Lazarus, 1993). All these simulations were performed for flat terrain (FT) conditions. Inclusion of high-resolution topography of an isolated mountain range in three-dimensional numerical models is not frequently found in literature (e.g. Smolarkiewicz and Clark, 1985; Carpenter and Droegemeier, 1998).

The effects of orography on cumulonimbus (Cb) cloud life are very complex in reality. Therefore, the numerical simulation of convective cloud under such conditions is of great practical and scientific interest. During the last decade, the new classes of cloud resolving mesoscale models have developed rapidly. They become capable to simulate the life cycle of individual convective clouds. Some papers (Lin and Joyce, 2001; Lin et al., 1998; Fovell and Tan, 1996) treated the propagation and cell regeneration within a multicell storm.

We focus our attention on an individual Cb cloud, which regenerates and propagates along a river valley following Čurić's (1982) results. The basic findings of his conceptual model based on numerous radar data and the observations on the ground are as follows: the Western Morava valley is important for the formation and propagation of isolated Cb clouds. If the ambient wind at low-level is roughly from SE direction (nearly parallel with a valley) and turns clockwise with altitude to NW direction, the cloud formed over the neighbour mountains will move down into the valley. A strong downdraft will occur during the cloud motion over the sloping mountainside before its passage along the valley. The propagation speed and the height, which periodically change in time, of the cold air nose (this term referred to the entire profile of the boundary between cold air and warmer environment) depend essentially on the relationship between pressure gradient force and surface friction (Čurić, 1980).

At the front part of the cold air nose, the daughter cloud can form. It contributes to the regeneration and faster cloud propagation along a valley because it is merged by the mother cloud. The apparent storm propagation speed attains 55 km/h, so that the advection of convective cells is much stronger than in some cases found in the literature (e.g. Lin et al., 1998).

Hereafter, we focus our attention to find out and analyze differences in a three-dimensional model clouds moving over complex terrain (CT) with a river valley and flat terrain if the other conditions are the same. We want to show whether an essential difference between these two cases exist. As a tool for affirmation of our statements, we use the cloud-resolving fully compressible mesoscale model.

2. Numerical simulations

The three-dimensional mesoscale model (ARPS) which generates the simulated cloud is described in detail by Xue et al. (2000, 2001). This model numerically integrates the time-dependent, nonhydrostatic and fully compressible equations. The turbulence is treated by 1.5-order turbulent kinetic energy formulation. The sound wave terms are integrated in time with a 2-s time step, while the other terms are computed with large time step of 6 s. The wave-radiating condition is used for lateral boundaries. For the top of the domain, the radiation condition is applied. The rigid bottom boundary is treated. In our calculations, we use the constant drag coefficients for momentum stress, turbulent heat flux and turbulent moisture flux at the ground surface. Differential heating of the valley slopes also takes into account. Coriolis force is neglected in our simulations.

The ARPS model uses a special case of the fully three-dimensional curvilinear coordinate system with coordinates (ξ, η, ζ) , since the constants ξ and η remain the same as those of constant x and y . The ζ is the terrain-following coordinate. The irregular grid associated with the curvilinear coordinate in the physical space is transformed to rectangular computational grid using standard procedure developed for Cartesian systems that consists of two steps: terrain-following coordinate transformation and vertical grid stretching.

The domain simulated by the model was $112 \times 112 \times 16 \text{ km}^3$ with a 1-km grid-spacing in the horizontal direction and 500 m in the vertical one. Our ARPS terrain preprocessor supports data sets 30×30 in. ($0.65 \times 0.65 \text{ km}^2$) covering Serbia and Montenegro with their

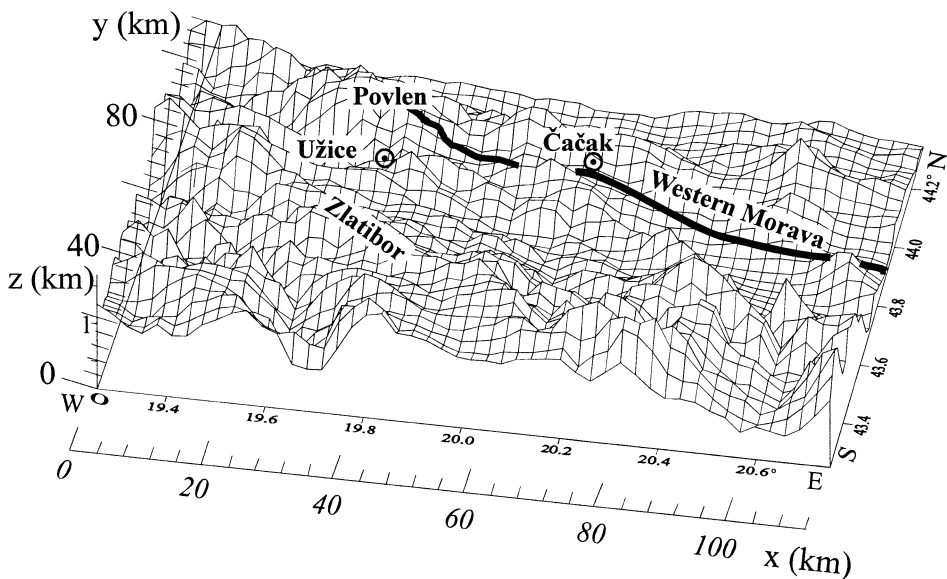


Fig. 1. Three-dimensional topography with the Western Morava valley within the model domain. Initial perturbation bubble center position is located over Povlen Mountain. The axes x , y and z are along the sidewalls of computational domain.

surroundings. The ARPS terrain preprocessing converts the original ASCII files into unformatted binary direct-access files. Later, these files are used for the creation of final smoothed terrain field. The three-dimensional terrain within the model domain is presented in Fig. 1 with its center at 43.8°N, 20°E. It represents the Western Morava valley (mean height above sea level 300 m) with its environment. The axes x, y and z are the sidewalls of computational domain. Horizontal homogenous model initial state using sounding is applied. The initial temperature, humidity and wind profiles are taken from the radiosonde data. The initial ellipsoidal bubble perturbation is expressed over potential temperature with the amplitude of 2 °C at $(x, y)=(32.96)$ km and 1.5 km over the mountain Povlen (the peak

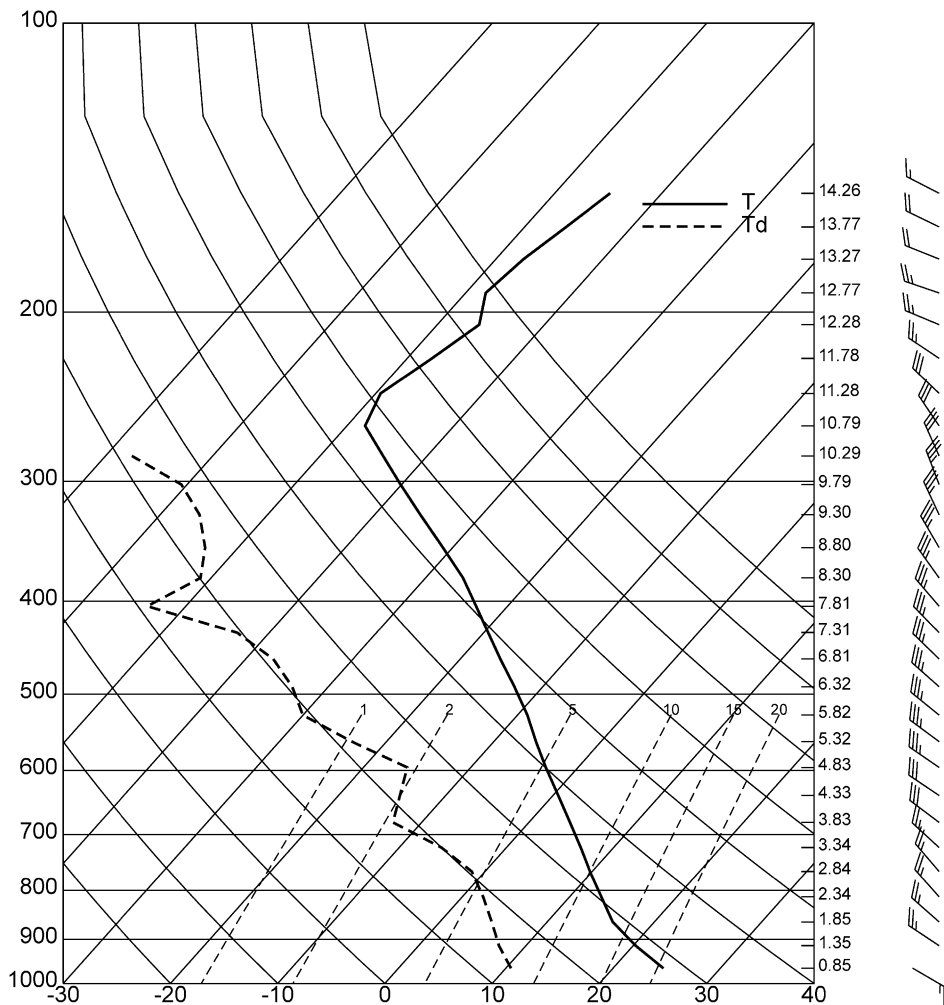


Fig. 2. Rawinsonde balloon sounding of 13 June 1982 at 10:00 of local time.

height is 1350 m) where $\zeta = 0$. The bubble dimensions are 10 km in horizontal and 1.5 km in vertical. The simulations were run for 120 min.

The model microphysical parameterization used is developed by Čurić and Janc (1993, 1997) and Čurić et al. (1999). It includes six categories of nonprecipitating and precipitating elements: water vapour, cloud water, rainwater, cloud ice, snow and hail. It differs from the other proposed bulk-water parameterizations in hail treatment. Our approach considers hail spectrum (called realistic hail spectrum) with only hail-sized particles (an equivalent sphere diameter equal and greater than 0.5 cm) instead of idealized hail spectrum (hail diameters are between 0 and ∞). As a consequence, the formulas for hail production terms are different from those given by Lin et al. (1983) because they also include the coefficients with incomplete gamma functions. Calculations show that the values of our hail production terms may differ from their earlier values by a factor of more than 3.

The impact of a valley terrain on Cb cloud evolution is analyzed through comparison of the simulated cloud characteristics under conditions of complex terrain (CT case) and flat terrain (FT case).

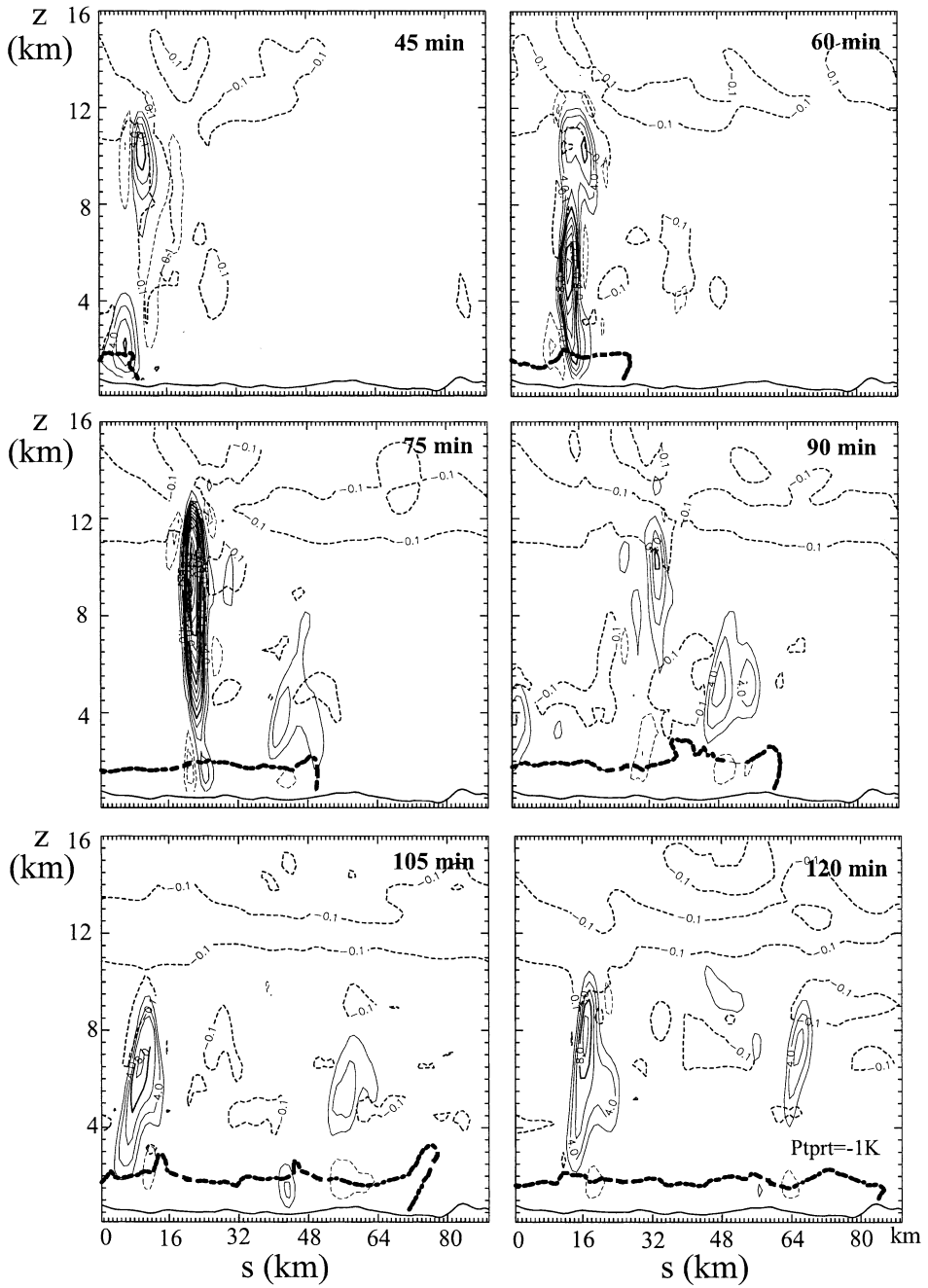
The sounding of 13 June 1982 at 10:00 local time with the corresponding wind profile is presented in Fig. 2. As noted, the wind direction veered sharply from southeast to northwest above 750 m (directional shear greater than 180°). The wind speed increased with altitude from around 7 m/s near the surface to about 17 m/s at 9 km MSL. Although the atmosphere is nearly stable and not too humid, the initial condition is favourable for individual Cb cloud development in accordance with Čurić (1982).

3. Experiments

We focus our attention to terrain effects on simulated storm dynamics. Therefore, we analyze the vertical velocity field in vertical cross-section through simulated cloud for both CT and FT cases along directions indicated in Figs. 7–9. The horizontal axis starts with 0 km at initial bubble center position.

Results of the CT case are presented in Fig. 3 for each 15-min intervals beginning at $t = 45$ min (t means simulated time). The model cloud moves towards the Western Morava valley after being initialized over Povlen mountain slopes at $t = 15$ min. We focus our attention to investigate the orography effects on the cloud in the valley.

Initially, the front-cell regeneration is not expressed over complex terrain (Fig. 3a) due to orography inhibition effects. Later on, the cold air nose is formed and the front-cell regeneration is clearly observed (vertical velocity maximum of over 18.7 m/s appears). The cold air nose height continues to grow considerably within the next time intervals, since the cold air fills the river valley flanked by mountainsides. In our considerations, we represent the cold air nose over perturbation potential temperature in accordance with Droegemeier and Wilhelmson (1987) and Rotunno et al. (1988). After cold outflow formation, this area is characterized by negative temperature perturbation and positive pressure one (e.g. Čurić, 1980, 1982). Perturbation potential temperature includes both of these effects. Generally speaking, the propagation speed of the cold air nose is associated with relatively frequent front-cell regeneration in the area flanked by mountainsides. At $t = 90$ min, the cold air nose has a “wave-like” shape (Droegemeier and



Wilhelmson, 1987). Near the ground, air turns downward due to the surface friction. Cell regeneration appears again if the local vertical velocity maximum, w_{\max} , is greater than 4 m/s. The other maximum at the backside of the mother cloud is associated with a new cell formed there. Within $t=15$ min, almost the whole integration domain in horizontal is filled by cold air. The local maximum (10.8 m/s) associated with a new formed cell is expressed, while the mother cloud decreases in its intensity. This is still more expressed for $t=120$ min. However, another front-cell regeneration still appears ($w_{\max}>4$ m/s). We can also observe that the vertical velocity maximum changes rather periodically, since the cold air nose tends to collapse and reform alternately.

The influence of the flat terrain is clearly expressed through the feature of vertical velocities (FT case; Fig. 4). For the first two time intervals ($t=45$ and 60 min), the front-cell regeneration is stronger than the CT case because the simulated cloud is not inhibited by orography effects. This inhibition for cloud development will be due to less supply of low-level moist air from the lateral direction into the cloud when it slides down the valley. On the other hand, this means also more intense processes beneath the cloud base. Updraft maximum is larger (23.5 m/s; Fig. 4a) than the CT case. Within the next time intervals, the front-cell regeneration appears at $t=120$ min ($w_{\max}>8$ m/s). After $t=45$ min, the cold air nose retards compared to the CT case due to the absence of cell regeneration in front of the mother cloud. The depth of the cold air nose is thinner especially at the backside because of the cold air divergence. Therefore, more time is needed for warm environmental air to be lifted over cold air nose.

Aforementioned characteristics come from observations and theory (Ćurić, 1980, 1982). The complex terrain of the Western Morava valley severely stimulates the storm propagation and cold air outflow in valley direction. Consequently, the cold air remains more compact in the valley. This is of an essential importance for the front-side cell regeneration of the mother cloud by forced lifting of warm moist air above the cold air nose. The front edge of the mother cloud is very close to the leading edge of the cold air outflow. The valley behind the cloud remains filled by cold air in which there is a considerable amount of moisture due to precipitation evaporation. After all, our experiments show that under given conditions, the front-cell regeneration is more frequent in the CT case than in the FT one.

The horizontal distribution of vertical velocity has not been considered yet. Therefore, we consider horizontal cross-sections of vertical velocity field for selected altitudes for the chosen time interval ($t=75$ min) when the model cloud attains strong intensity. For the CT case (Fig. 5), two cells at flank sides of the mother cloud propagate nearly to 10 km in height. The cell formed in front of the mother cloud is well expressed to 8 km (it is indicated by dark arrow at each figure), with tight zone of downward motions ahead. This

Fig. 3. Time sequence of vertical cross-sections of vertical velocity fields (contour interval of 1 m/s) through simulated storm in the valley for the CT case and 15-min intervals beginning at 45 min of simulated time. Solid and dash lines denote upward and downward motions, respectively. The cold air nose is depicted with bold solid line with -1 K perturbation potential temperature. The horizontal axis (s) is along the Western Morava valley orientation. Its location within computational domain is indicated in Figs. 7–9. The horizontal axis starts with 0 km at initial bubble center position. All distances are in kilometer.

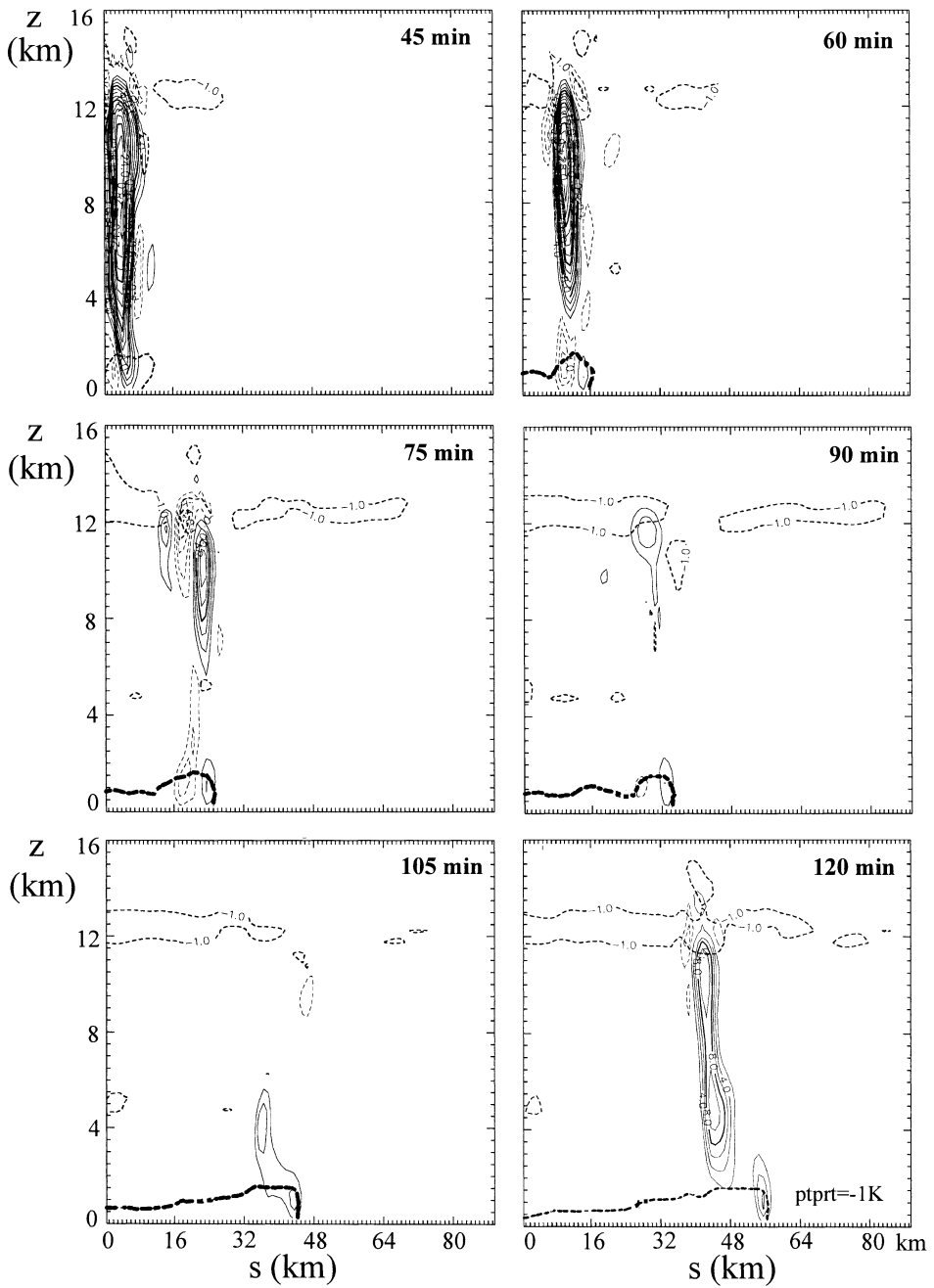


Fig. 4. As in Fig. 3, but for the FT case.

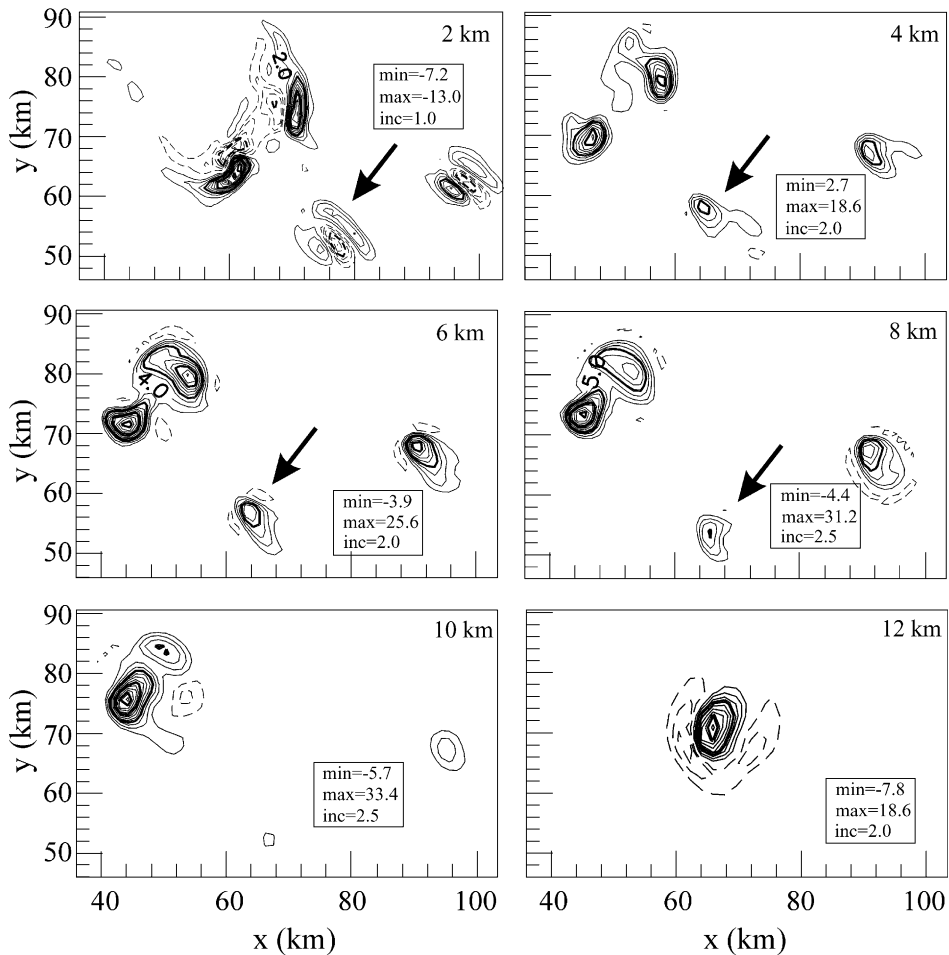


Fig. 5. Horizontal cross-sections of vertical velocity field for altitudes between 2 and 12 km with 2 km step at $t = 75$ min for the CT case within computational domain. Extreme values and increment of vertical velocity are given at each plot. The arrow denotes a cell formed at front-side of the mother cloud. All distances measured along x - and y -axes are in kilometer.

is caused by the next processes: fast propagation of both the mother cloud (~ 45 km/h) and the cold air nose; warm air lifting strongly upward above the leading edge of the cold air. The cell at the right flank of the cloud is much stronger (33.4 m/s) than that at the left flank. Behind them, compensating downward motions exist. In contrast, none of the cells at the front part of the mother cloud is for the FT case (Fig. 6). Two cells at cloud flanks are more intense (38.8 m/s at $z = 10$ km; cell at the right flank) and they also encircle considerably larger areas than in the CT case for all selected altitudes. This results from the fact that the cloud development is then not inhibited in the lateral direction. At $z = 12$ km, it exists only in one cell at the right flank of the cloud.

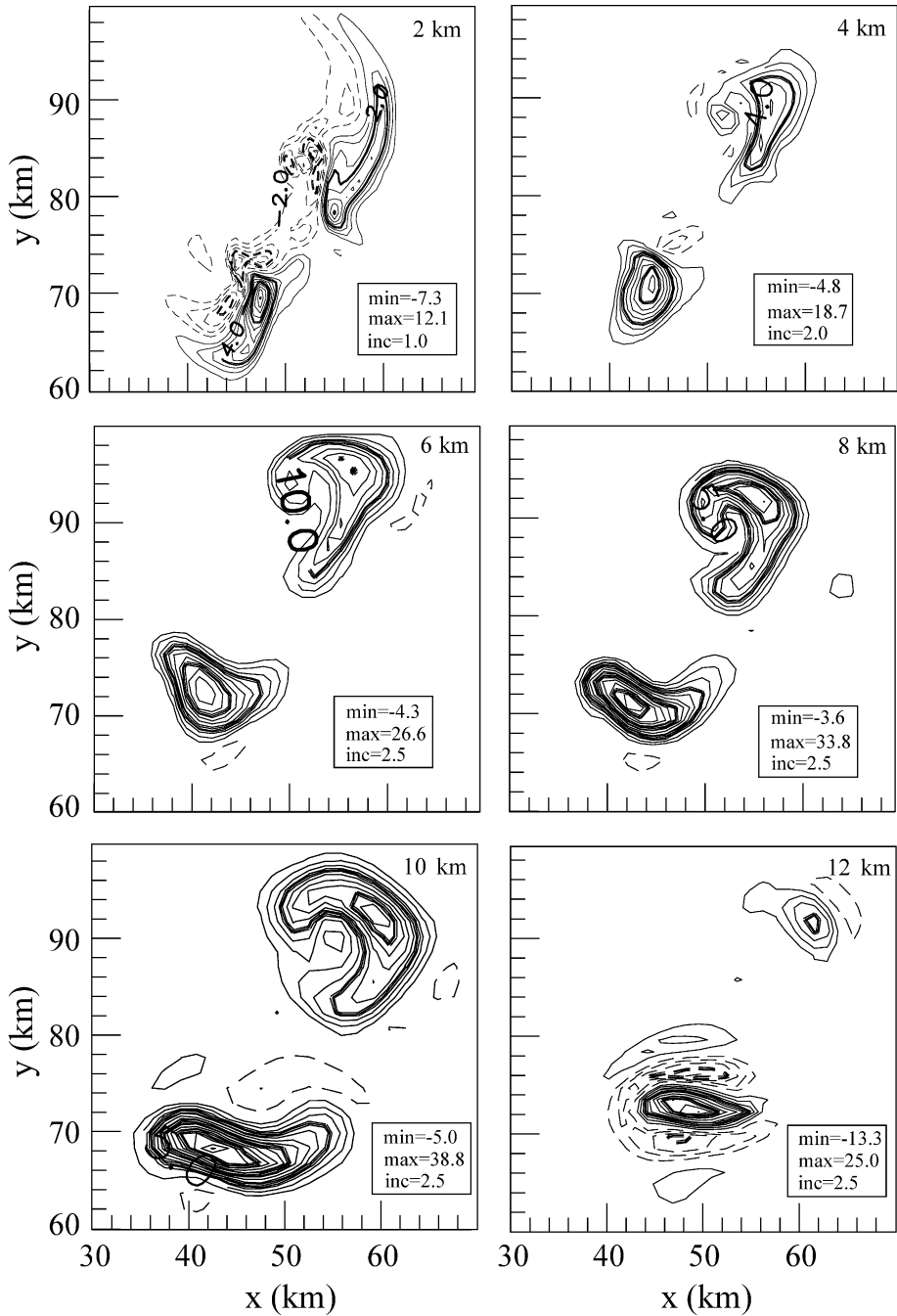


Fig. 6. As in Fig. 5, but for the FT case.

From Figs. 5 and 6, cells at both flanks of the storm are well expressed at discrete altitudes. We are also interested to consider the three-dimensional visual appearance of cell tubes for both CT and FT cases. Cell tubes have smaller cross-section areas for the CT case (Fig. 7a) than for the FT one (Fig. 7b). This is caused by the valley terrain effects. The CT case also shows that the cell at the left flank is more tilted compared to the environmental shear than at the right flank.

Our insight in terrain influence on cloud characteristics would be more complete if we consider maximum areas of cold air beneath the cloud base (grey-coloured area; -1 K is an isoline of perturbation potential temperature) and rain precipitation zone (black-coloured area, an isoline of 0.01 g/kg of rain water mixing ratio) at $\zeta=0$ for both CT and FT cases (Figs. 8 and 9). From the figures, we can also see the cloud position within the integration domain. Dimensions are the same as in Fig. 1. Results show the expected feature: the precipitation zone is overlapped with the front part of cold air outflow, since downwards motion is well correlated with evaporating precipitation elements within it (e.g. Čurić, 1982). Initially, the precipitation area does not differ a lot from that of the cold

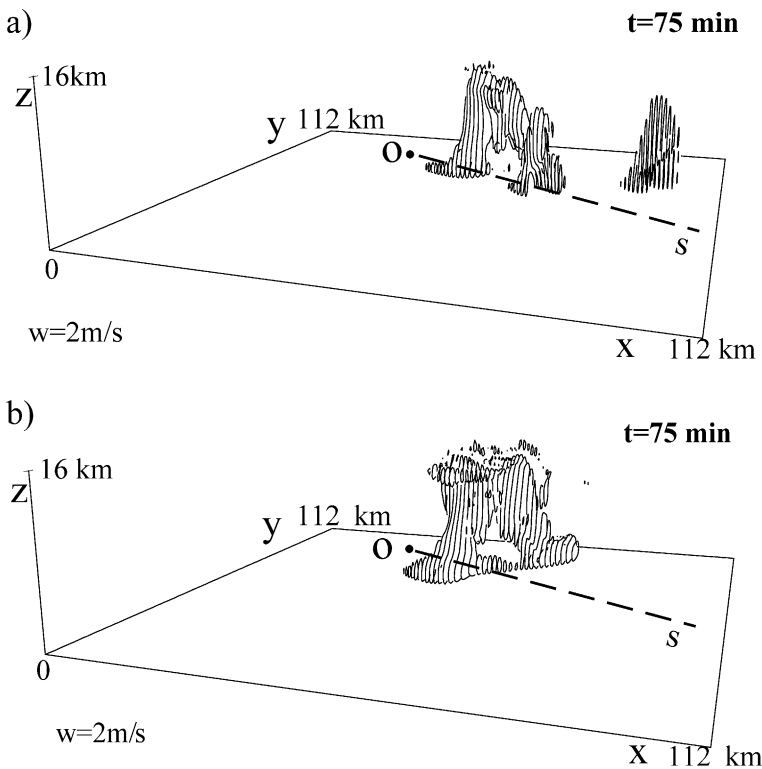


Fig. 7. Fields of vertical velocity (values equal or greater than 2 m/s) for (a) CT and (b) FT case at $t=75\text{ min}$. Axes x , y and z are along the sidewalls of computational domain, while s -axis (dash line) is also shown. The point “O” denotes the initial bubble center position.

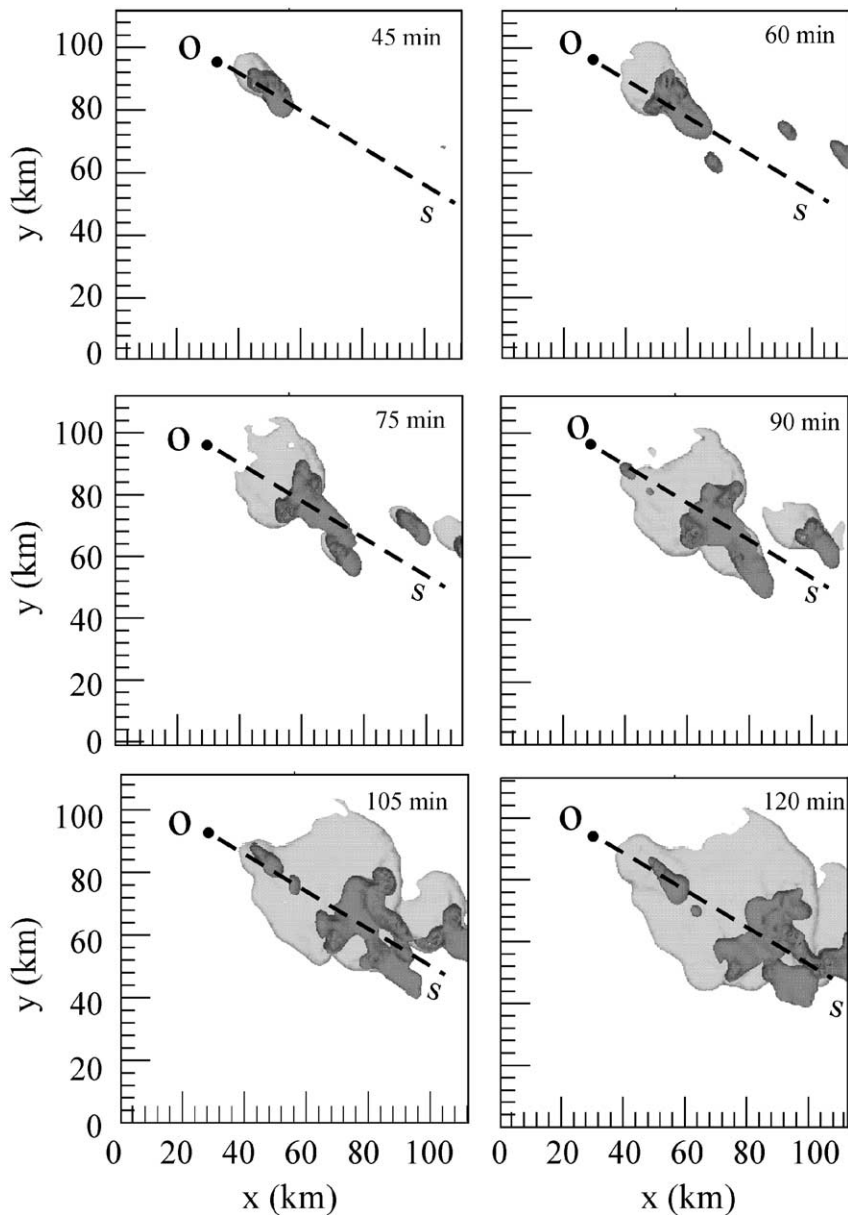


Fig. 8. Horizontal cross-sections of the cold air dome (gray-coloured area; -1 K perturbation potential temperature isoline) and the rain precipitation area (black-coloured area; 0.01 g/kg of rainwater mixing ratio isoline) at $\zeta=0$ for the CT case and the same time intervals as in Fig. 3. The dashed line (s -axis) indicates the location of the vertical cross-section. It is along the Western Morava valley orientation. The other two axes (x and y) are along the sidewalls of computational domain. All distances are in kilometer.

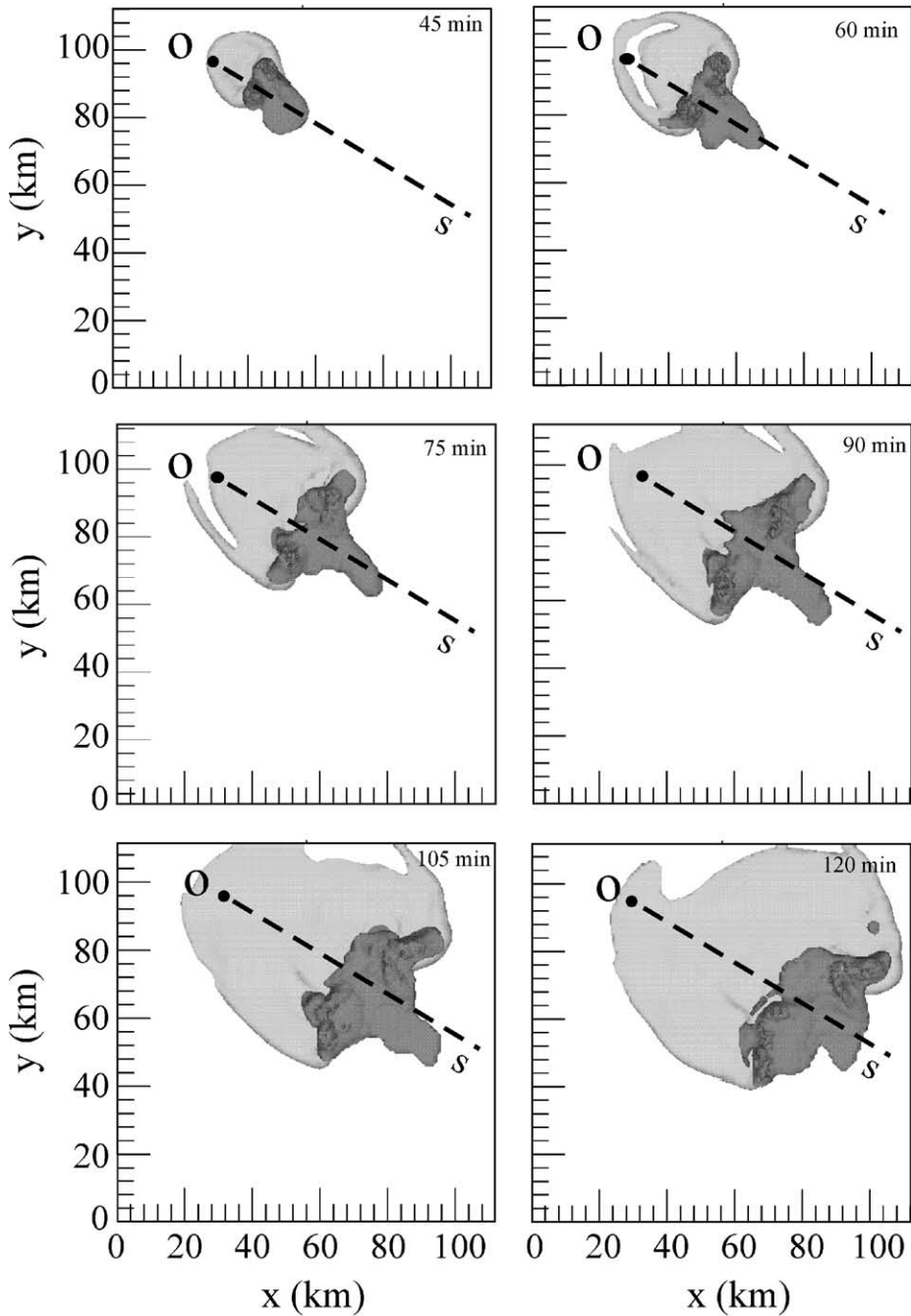


Fig. 9. As in Fig. 8, but for the FT case.

air outflow. After it, the cold air remains behind the precipitation zone. Both considered areas spread predominately along the river valley, while their propagation in the lateral direction is inhibited by the valley sides (Fig. 8). After $t=105$ min, another smaller precipitation area appears at the backside of cold air outflow area. This is associated with a new cell formed behind the mother cloud. For the FT case (Fig. 9), the cloud growth is not inhibited by orography effects, so that both the rain precipitation and cold air outflow will encircle larger horizontal area.

Different growth stages of simulated cloud and the relative position of cold air nose can be observed from its visual appearance in vertical cross-section (Fig. 10). Hereafter, we present the contour of the total cloud field (cloud water and ice with threshold of 0.01 g/kg, rainwater and hail with threshold of 0.1 g/kg and snow with threshold of 0.06 g/kg). This model appearance has no characteristic anvil, which propagates in the front-side of the cloud in downward direction. Cloud feature shown is due to the relatively high threshold used for cloud ice mixing ratio. By lowering the

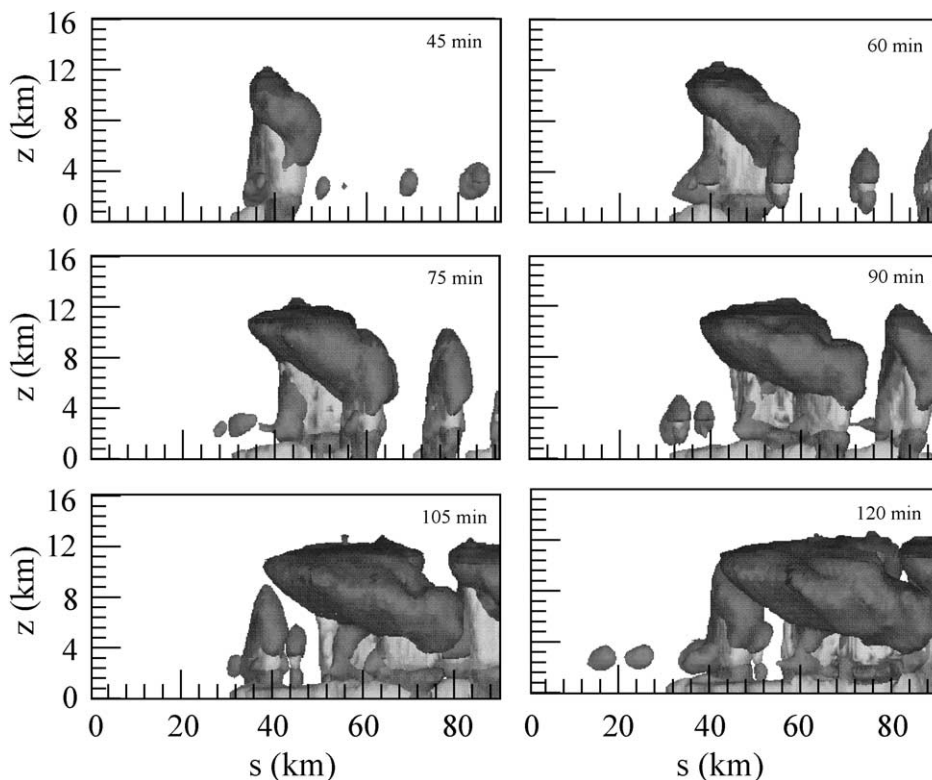


Fig. 10. Visual appearance of total cloud field (0.01 g/kg cloud water or cloud ice mixing ratio isoline; 0.1 g/kg for rainwater or hail mixing ratio isoline and 0.06 g/kg for snow mixing ratio isoline) given in vertical cross-section along s -axis (the Western Morava valley orientation) for the CT case. Gray-coloured region below the cloud base represents the cold air dome. All distances are in kilometer measured along s -axis.

corresponding threshold for cloud ice, it would block the view of the other contents. As noted, the leading edge of the cold air nose supports our presumption that it lies close to the front part of the mother cloud. The front-cell regeneration mechanism is well expressed. The cell formed northeasterly from the mother cloud grows intensely after $t=75$ min. Another cell formed behind the mother cloud develops and tends to merge by it. The model cloud for the FT case shows different visual appearance (Fig. 11). It is more developed in agreement with more intense growth in this case. No new cell is formed here.

We have noted that the front-cell regeneration is less expressed for the FT case than for the CT one in considered vertical cross-section. In contrast, the cloud intensity is greater for the FT case due to the absence of lateral orography inhibition. Finally, we present the absolute maximum of vertical velocity (its value and height) as an important indicator of cloud development intensity. Time evolutions of both parameters are shown in Fig. 12. As noted, these characteristics are always greater in magnitude for the FT case than for the CT one (the greatest value of 45 m/s at $z=10.5$ km and $t=60$ min in

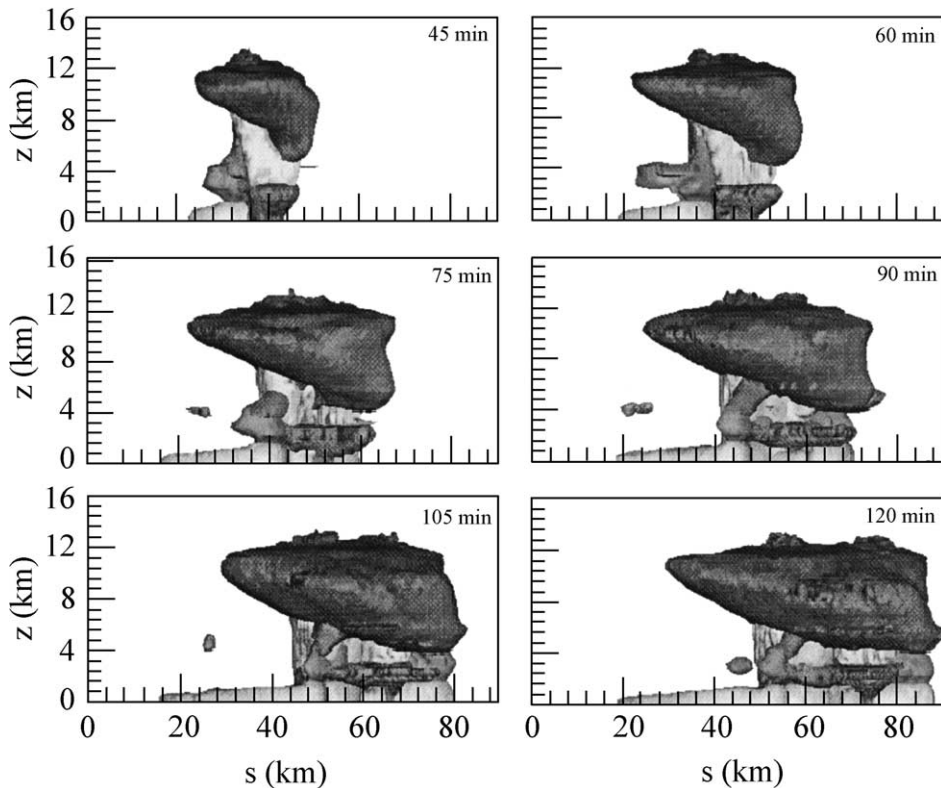


Fig. 11. As in Fig. 10, but for the FT case.

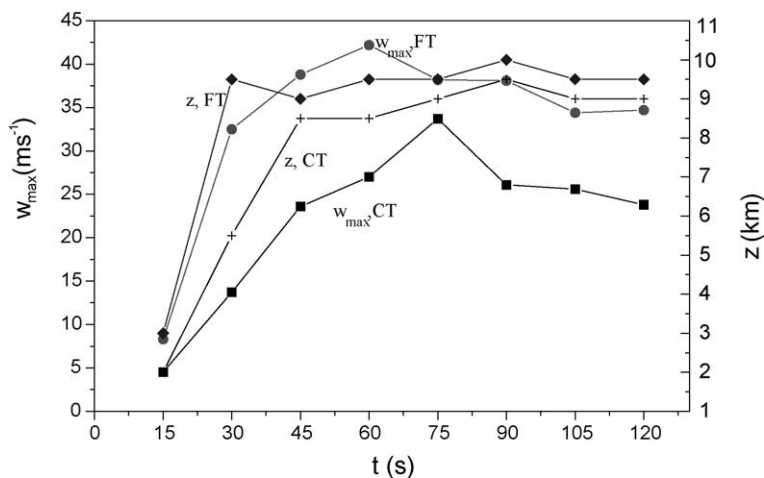


Fig. 12. Absolute maximum of vertical velocity, w_{\max} (in m/s), versus time (in min) for the CT case (line with black-coloured squares) and the FT case (line with black-coloured circles), respectively. Height of this maximum, z (in km), as a function of time is presented by the lines with crosses (CT case) and black-coloured rhombs (FT case), respectively.

contrast with 36 m/s at $z=9.4$ km and $t=90$ min). This means that the cloud over flat terrain attains its maximum intensity within a shorter time interval.

4. Conclusions

The model characteristics of an isolated Cb cloud moving along a valley give us the full insight in nature of such cloud and the orographic impact on its life cycle. The summaries of our findings concerning the intercomparison of the two cases (CT and FT) are as follows:

- It is found that the orography effects (CT case) make the simulated cloud more compact compared to the FT case. This is due to the fact that the Cb cloud development is inhibited by the less supply of low level moist air from the lateral direction into the cloud. Such orography influence on Cb cloud development is a characteristic in this special case when the cloud slides down the valley. In other cases, as it is well known, the orography enhances convection over the mountains. Therefore, the simulated cloud over flat terrain is more intense with greater magnitude of the absolute vertical velocity maximum that appears at higher levels.
- Beneath the cloud base, a cold air nose is formed. Under orography conditions, it is also more compact taking greater depth. Warm environmental air lifting aloft over the cold air nose is then more frequent leading to faster Cb cloud propagation along a valley compared to the FT case. Front-cell regeneration also appears after longer time interval for the flat terrain due to the absence of orography effects. In addition, reform and collapse of the cold air nose are more expressed in the CT case.

To conclude, a cloud-resolving model like ARPS seems to be a powerful tool for the simulation of Cb clouds in complex terrain conditions.

Acknowledgements

This research was supported by the Ministry of Science, Technology and Development of Serbia through the Project “Extreme weather events in Serbia”. Two anonymous reviewers have made many suggestions in the reviewing processes that increased the completeness and clarity of this paper. Their contributions are appreciated.

References

- Carpenter Jr., R.L., Droegemeier, K.K., 1998. Entrainment and detrainment in numerically simulated cumulus congestus clouds: Part I. General results. *Atmos. Res.* 55, 3417–3432.
- Ćurić, M., 1980. Dynamics of a cold air outflow from the base of the thunderstorm. A simple model. *J. Rech. Atmos.* 14, 493–498.
- Ćurić, M., 1982. The development of the cumulonimbus clouds which moves along a valley. In: Agee, E.M., Asai, T. (Eds.), *Cloud Dynamics*. Reidel, Dordrecht, pp. 259–272.
- Ćurić, M., Janc, D., 1993. Predictive capabilities of a one-dimensional convective cloud model with forced lifting and a new entrainment formulation. *J. Appl. Meteorol.* 32, 1733–1740.
- Ćurić, M., Janc, D., 1997. On the sensitivity of hail accretion rates in numerical modeling. *Tellus* 49A, 100–107.
- Ćurić, M., Janc, D., Vučković, V., 1999. Verification of the improved predictive capability of a 1-D forced time-dependent cloud model with truncated hail spectrum. *Meteorol. Z., N.F.* 8, 143–154.
- Droegemeier, K.K., Lazarus, S.M., 1993. The influence of helicity on numerically simulate convective storms. *Mon. Weather Rev.* 121, 2005–2029.
- Droegemeier, K.K., Wilhelmson, R.B., 1987. Numerical simulation of thunderstorm outflow dynamics: Part I. Outflow sensitivity experiments and turbulence dynamics. *J. Atmos. Sci.* 44, 1180–1210.
- Fovell, R.G., Tan, P.-H., 1996. Why multicell storms oscillate. 18th Conf. Severe Local Storms. Amer. Meteor. Soc, San Francisco, CA, pp. 186–189. Preprints.
- Klemp, J.B., Wilhelmson, R.B., 1978. The simulation of three-dimensional convective-storm dynamics. *J. Atmos. Sci.* 35, 1070–1096.
- Lin, Y.-L., Joyce, L.E., 2001. A further study of mechanisms of cell regeneration, development and propagation within a two-dimensional multicell storm. *J. Atmos. Sci.* 58, 2957–2988.
- Lin, Y.-L., Farley, R.D., Orville, H.D., 1983. Bulk parameterization of the snow field in a cloud model. *J. Clim. Appl. Meteorol.* 22, 1065–1092.
- Lin, Y.-L., Deal, R.L., Kulie, M.S., 1998. Mechanisms of cell regeneration, propagation, and development within two-dimensional multicell storms. *J. Atmos. Sci.* 55, 1867–1886.
- Rotunno, R., Klemp, J.B., Weisman, M.L., 1988. A theory for strong, long-lived squall lines. *J. Atmos. Sci.* 45, 463–485.
- Smolarkiewicz, P.K., Clark, T.L., 1985. Numerical simulation of the evolution of a three-dimensional field of cumulus clouds: Part I. Model description, comparison with observations and sensitivity studies. *J. Atmos. Sci.* 42, 502–522.
- Toutenhoofd, V., Klemp, J.B., 1983. An isolated cumulonimbus observed in northeastern Colorado: comparison of field observations with results of a three-dimensional simulation. *Mon. Weather Rev.* 111, 468–478.
- Xue, M., Droegemeier, K.K., Wong, W., 2000. The Advanced Regional Prediction System (ARPS)—a multi-scale nonhydrostatic atmospheric simulation and prediction model: Part I. Model dynamics and verification. *Meteorol. Atmos. Phys.* 75, 161–193.
- Xue, M., et al., 2001. The Advanced Regional Prediction System (ARPS)—a multi-scale nonhydrostatic atmospheric simulation and prediction model: Part II. Model physics and applications. *Meteorol. Atmos. Phys.* 76, 143–165.